Closed-loop control of intense-laser fragmentation of S_8

E. Wells,[1,2] K. J. Betsch,[2] C. W. S. Conover,[3] Merrick J. DeWitt,[4,*] D. Pinkham,[1] and R. R. Jones[1,†]
[1]*Department of Physics, University of Virginia, Charlottesville, Virginia 22904-4714, USA*
[2]*Department of Physics, Augustana College, Sioux Falls, South Dakota 57197, USA*
[3]*Department of Physics and Astronomy, Colby College, Waterville, Maine 04901, USA*
[4]*Department of Chemistry, University of Virginia, Charlottesville, Virginia 22904-4319, USA*
(Received 9 August 2005; published 6 December 2005)

A liquid-crystal-based, laser-pulse shaper has been used in combination with an adaptive genetic feedback algorithm to investigate closed-loop control of intense laser fragmentation of S_8 molecules. We observe that the yield ratios $S_N^+:S_M^+$, for the production of specific charged fragments S_N^+ and S_M^+, can be enhanced by $>300\%$ relative to those observed using transform-limited 150-fs laser pulses. We have explored the effectiveness of time- and frequency-domain pulse parametrizations while shaping either (i) only the spectral-phase distribution or (ii) the spectral-phase and amplitude distributions of the light. We find that pulse complexity, requiring control beyond simple manipulation of the peak pulse intensity and duration, is critical for optimizing the yield ratios for most species. The "optimum" pulse shapes obtained using different pulse parametrizations show significant differences while yielding similar signal enhancements. In some cases, comparison of the different optimum pulse shapes appears to be a useful method for identifying pulse traits that are, or are not, important for manipulating a particular yield ratio. The importance of specific traits in the optimum pulse shapes is also explored numerically using principal control analysis. We conclude that closed-loop control can be effective for optimizing highly nonlinear strong-field processes. However, in general, intensity variations in a focused laser beam severely limit one's ability to associate the optimization results with specific dynamical mechanisms that bear primary responsibility for the control.

DOI: 10.1103/PhysRevA.72.063406 PACS number(s): 33.80.Rv, 42.50.Hz, 34.50.Gb

I. INTRODUCTION

When molecules or clusters are subjected to extremely intense laser fields, both ionization and fragmentation can occur. In some applications—e.g., mass spectrometry, it is desirable to produce only the parent molecular ion or specific charged fragments [1–4]. Not surprisingly, the ionizing laser's color, intensity, and/or temporal structure can often be adjusted to manipulate the relative yield into particular fragments. However, due to the complexity of these systems, it is not generally possible to know *a priori* the specific laser characteristics that will maximize the desired yield for a particular target. Therefore, laser-pulse shapers [5,6] and feedback algorithms [7–9] have recently been employed to control the relative fragmentation yields in large molecules [10–12].

Here we report on a recent investigation of closed-loop control of intense laser ionization and dissociative ionization of S_8 molecules. These crown-shaped sulfur rings provide interesting targets for control experiments. In particular, they are atomically homogeneous with high spatial symmetry. In addition, the ionization potentials (IP's) of the species, S_N $(1 \leqslant N \leqslant 8)$, are similar, 9.5 ± 1 eV [13]. Thus, there is no clear "handle" or "knob" for manipulating the branching ratio for photofragmentation into the different ionic channels. Through these measurements we seek answers to the following questions. Can the specific nonperturbative processes that lead to dissociation and/or ionization in the S_8 system indeed be controlled? Can we use our successes (and failures) in controlling this system to better understand closed-loop optimization of strong-field processes in general? How does one best formulate fitness functions to allow for moderate controllability while finding robust solutions in the presence of experimental noise [14–16]? What are the advantages, if any, of using specific laser pulse parametrizations (e.g., time or frequency domain) in an optimization experiment [9,17]? Should we expect the optimum pulse shapes to provide physical insight into the fragmentation mechanism [18–20]?

II. EXPERIMENT

To perform the experiments, sulfur powder is placed in an open Pyrex beaker in a vacuum chamber with a background pressure of approximately 10^{-7} Torr. At room temperature the sulfur vapor is composed primarily $(\sim 80\%)$ of S_8 molecules. The vapor also contains S_6 $(\sim 15\%)$ and essentially negligible amounts of other stable sulfur species S_N [21]. The amplified output of a mode-locked Ti:sapphire laser is focused into the sulfur vapor between two parallel field plates in a time-of-flight (TOF) mass spectrometer. A voltage applied to the lower field plate produces a uniform static electric field that pushes photoions produced by the laser toward a microchannel plate (MCP) detector. Molecular ions with different charge:mass ratios are distinguished by their TOF. We observe the production of positive ions only. When the extraction fields on the spectrometer and MCP are configured

*Current address: SPARTA, Inc., 1911 N. Fort Myer Drive, Suite 1100, Arlington, VA 22209, USA.
†Electronic address: rrj3c@virginia.edu

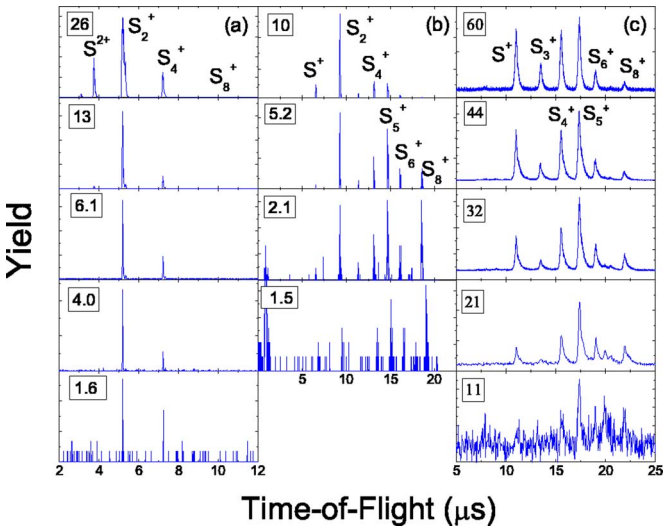

FIG. 1. (Color online) The time-of-flight mass spectrum of S_8 under various laser conditions. Column (a) is for 800-nm, 1-ps pulses. Column (b) is for 790-nm, 150-fs pulses. Column (c) is for 790-nm, 35-fs pulses. The number in the box of the upper left of each time-of-flight spectrum is the peak laser intensity in units of 10^{11} W/cm^2. Yields have been normalized to the dominant peak in each plot. Typically, the yield at the lowest laser intensity is approximately 50 000 times less than the most intense conditions shown in that column.

to detect negatively charged particles, electrons but no negative ions are observed. Apparently, the probability of negative-ion production is negligibly small. This may or may not be the case for neutral fragments. We cannot detect neutral particles with our current experimental configuration. Moreover, our measurements do not enable us to determine whether specific ion fragments are formed directly through dissociative ionization or indirectly via multiphoton ionization of neutral fragments.

In principle, the ion signal in a particular TOF peak may contain contributions from ion fragments with different masses and different charge states. However, the absence of significant levels of S_1^{2+} in the TOF signal indicates that singly, rather than multiply charged species, dominate the ion spectrum at the relatively low laser intensities ($<10^{13}$ W/cm^2) used in the experiments. Furthermore, under the assumption that ionization occurs much more rapidly than dissociation, the presence of charge-asymmetric channels (such as $S_8^{2+} \rightarrow S_1^{2+} + S_7$) in the fragmentation branching ratio is unlikely. In addition, previous measurements [22] of intense field ionization of S_2 at 5×10^{12} W/cm^2 do not show S_1^+ or S_1^{2+} production. Thus, given the uniformity in the IP's for the species S_N, since S_1^{2+} is not observed in the current experiment and S_1^+ production from S_2 is not observed under similar pulse conditions, it is unlikely that multiple ionization of S_8 or its daughter fragments occurs at a significant level.

As shown in Fig. 1(b), with low-intensity (10^{11} W/cm^2) unshaped 150-fs pulses, essentially all singly charged fragments S_N^+ are seen, but the parent molecular ion S_8^+ is responsible for the largest peak in the spectrum. With increasing intensity, smaller fragments are produced with higher efficiency. Near 10^{12} W/cm^2, S_2^+ fragments dominate the spectrum. At much higher intensities $>10^{13}$ W/cm^2, fragmentation is complete and only atomic ions S_1^+ and S_1^{2+} are seen. If the maximum pulse intensity is held fixed while the pulse length is increased, either by chirping the pulse or restricting its bandwidth, lower-mass species are produced with increased efficiency. With 1-ps pulses, as shown in Fig. 1(a), S_2^+ fragments dominate the spectrum for intensities as low as 10^{11} W/cm^2 and as high as 10^{12} W/cm^2. At intensities well in excess of 10^{12} W/cm^2 atomic ion fragments appear and eventually become predominant. Conversely, measurements with 35-fs pulses [Fig. 1(c)] show that at intensities well above 10^{12} W/cm^2, many larger fragments survive the laser pulse.

Clearly the relative yields into different charged fragments change as the laser intensity and/or pulse duration is varied. However, the control afforded by tuning only these parameters is quite coarse, and the variation in the yield ratios for different species often comes at the expense of total yield. In an attempt to achieve finer control with higher yields, we enabled a closed-loop optimization [7] of the laser parameters using a genetic algorithm (GA) [8,23] and liquid-crystal-based pulse shaper. The pulse shaper spatially separates the spectral components of the laser field, and the liquid crystal (LC) alters the amplitude and phase of the light within the frequency window associated with each LC pixel [5,6]. Using the experimental results as feedback, we employ the GA to search for a set of laser pulses that best achieve some defined target associated with the measured fragmentation branching ratio—e.g., maximize the signal in a particular S_N^+ fragment channel or minimize the production of fragments with $N<4$, etc. The search algorithm specifies a "genetic code" for each laser pulse, or "individual." To begin the search, a "generation" of 50 or so individuals is created from random genetic sequences. The fitness of each individual in the generation is assessed according to its performance in achieving the specified target goal. A second generation of individuals is produced based on the genes of "mated" pairs of individuals from the first generation. Our algorithm uses tournament selection to determine which individuals are allowed to reproduce. Individuals with higher fitness have a greater chance of being selected for reproduction. We use single-point crossover of the parent chromosomes and a moderate ($\sim 1\%$ per bit) mutation rate to determine the genetic code of offspring. We also add a genetic copy of the fittest adult into the next generation to ensure that the best performance in the second generation is at least as good as that in the first. The fitness of the individuals in the second generation is then assessed, and the process is repeated through the performance of successive generations until the GA converges on a solution.

For most of the experiments described in this article, the GA was programmed to maximize a ratio $S_N^+ : S_M^+$ for specific fragment masses M and N. Care was taken to select robust fitness functions that prevented the GA from settling on a solution that simply decreased the yield of both the numerator and denominator of the ratio, resulting in an undefined fitness of $\frac{0}{0}$. The addition of a small positive constant offset to the denominator yield ensures that laser pulses that produce little or no total ion yield result in low fitness. Set-

ting the offset to 10% of the S_M^+ yield obtained with unshaped pulses works well as it places a significant penalty on solutions with low numerator signals. We find that larger offsets allow the algorithm to find solutions even in the presence of experimental noise, but make it impossible for the algorithm to appreciate the best solutions where the denominator signal is near zero. Conversely, smaller offsets, which in principle allow the algorithm to more easily find solutions with zero-denominator-yield signal, are unstable.

As described in more detail below, we use either time- or frequency-domain code parametrizations where the genes specify particular aspects of the time or frequency dependence of the field, respectively. Of course, in either case, the genetic code is manifest as the application of different voltage levels to each of 256 pixels in the LC. The laser amplifier runs at a 1-kHz repetition rate, but the LC requires approximately 1/2 second to update its voltages and create a different individual. Therefore, to simultaneously optimize the signal-to-noise ratio and our data-collection efficiency, the LC is set to produce the same individual for several thousand identical laser shots. We use boxcar integrators to measure the average signal in the TOF peaks of interest during each averaging period. Data collection pauses when new voltages are loaded into the LC.

We monitor every individual pulse shape by directing a fraction of the light in each laser pulse into a polarization-gated, frequency-resolved optical-gating (PG FROG) device [24]. Spectrogram data obtained from the PG FROG can be inverted to obtain the time-dependent field in each laser pulse. Prior to the experiments, the voltage-dependent retardance of the LC pixels was calibrated and the PG FROG was used to verify successful programming of a variety of pulse shapes and pulse sequences including: single transform-limited pulses, linearly chirped pulses, two identical pulses with a defined relative delay, pulses with sinusoidal phase modulation, etc. To reduce the amount of data generated during the GA optimization, PG FROG spectrograms are saved only for the "optimum" pulse shapes in each experiment. However, the gene sequence for each trial individual in every generation is recorded. By using the LC calibration we can, with reasonable accuracy, infer the time-dependent field for each individual.

III. RESULTS AND DISCUSSION

Most of our efforts have focused on optimizing simple yield ratios $S_N^+:S_M^+$ with $1 \leqslant (N,M) \leqslant 8$. The results of the 81 optimization experiments we performed are summarized in Table I. The rows and columns (labeled 1–8) in the table correspond to N and M for an optimized $S_N^+:S_M^+$ ion ratio. Each numerical entry in the table is a ratio of ratios, $[S_N^+:S_M^+]_{best}/[S_N^+:S_M^+]_{unshaped}$, for a distinct experiment. The diagonal entries $[N,N]$ in the table represent absolute yield ratios $[S_N^+]_{best}/[S_N^+]_{unshaped}$. The superscripts (1, 2, 3, or 4) preceding each entry indicate the pulse parametrization scheme and shaping methods used for the particular experiments. Specifically, experiments of type 1 and type 2 use a frequency-domain pulse parametrization with (1) phase-only or (2) phase and amplitude shaping, respectively. Type 3 and type 4 measurements utilize a time-domain pulse parametrization with (3) phase-only or (4) phase and amplitude shaping, respectively.

The details of the different optimization schemes and a more focused look at the results of several of the experiments are presented below. However, at this point it is worth noting several key features of the experiments that are clearly illustrated by the results in Table I. First, intense laser fragmentation of S_8 can indeed be controlled using the closed-loop scheme. In spite of the fact that the first generation of laser pulses are built from random genetic codes, use of the GA results in a significant enhancement in the ratio of interest, almost invariably through a large reduction of the denominator-ion yield with less or no reduction in numerator-ion signal. This is not *a priori* obvious given the nonlinear intensity dependence of the dissociative ionization processes and the experimental integration of ion signal originating from different intensity regions throughout the laser focal volume. Second, the effectiveness of the GA is roughly independent of the gene parametrization scheme used for the optimization. However, as we discuss in more detail below, the "fittest" individuals found with the different schemes exhibit significant differences. Examination of these differences and the implementation of principal control analysis makes it possible to identify spectral and/or temporal features which are, or are not, critical for control of specific ratios. Detailed studies using four different parametrization methods were performed on a small number of target products. The results described in the following paragraphs focus on the $S_1^+:S_2^+$ and $S_2^+:S_1^+$ yield ratios.

In one set of experiments, the GA is operated using a common frequency-domain parametrization [8,11], where the "genes" that determine the laser-pulse shapes are expressed directly as the phase (type 1) or phase and amplitude (type 2) of the laser light at different positions within the spectral bandwidth. Typically, the search space is reduced to a maximum of 32 genes by constraining groups of adjacent LC pixels such that they do not vary independently. This improves the speed and convergence of the algorithm [9], but it also severely restricts the types of laser pulses that can be produced. Importantly, for fragmentation of large species such as S_8, a key molecular rearrangement may require that the laser pulse have structure over times scales of several picoseconds or more. Such pulses are not obtainable using the standard pixel clustering method since longer time features require finer spectral resolution. In addition, grouping adjacent pixels can introduce a natural spectral periodicity, resulting in modulations in the temporal field amplitude. This significantly limits our ability to determine whether specific temporal or spectral features in the best pulse appear because the molecule prefers them or because of an artifact due to pixel clustering. Indeed, as shown in Figs. 2–4, the optimized pulses for $S_1^+:S_2^+$ and $S_2^+:S_1^+$ show significant temporal modulations that are different for the two target ratios, but are consistent for type-1 and type-2 shaping.

Based on our measurements with unshaped pulses, shown in Fig. 1, it is clear that smaller fragments are more easily produced with longer pulses and/or higher intensities. The optimum pulse shapes found by the GA suggest the same dependence. For example, with phase-only shaping (type 1),

TABLE I. Closed-loop optimization results for various ratios $[S_N^+:S_M^+]_{best}/[S_N^+:S_M^+]_{unshaped}$, where N and M are the masses of the fragment ions. The diagonal entries $[N,N]$ represent absolute yield ratios $[S_N^+]_{best}/[S_N^+]_{unshaped}$. The superscript prior to each number indicates the type of pulse parametrization, as described in the text. The numbers in bold represent the highest fitness for that particular experiment and pulse parametrization scheme. No significant yield of S_7^+ was observed in any experiment. Only 11 of 81 experiments failed to achieve a ratio of greater than 1.0—i.e., a fitness greater than that of the unshaped pulse.

	$M=1$	$M=2$	$M=3$	$M=4$	$M=5$	$M=6$	$M=8$
$N=1$		^{1}0.53^{1}2.2^{1}1.0					
		^{1}1.4^{1}1.8^{1}4.5					
		^{1}**5.3**^{1}3.5^2**3.0**					
		^{2}2.8^{4}1.4^4**2.7**					
		^{3}2.1^{3}2.2^3**3.3**					
		^{3}2.7^{3}1.2^{3}1.3					
		^{3}2.5					
$N=2$	^{1}1.5^1**3.2**^{1}2.2	^{1}1.1^1**1.2**^{1}0.85		^{4}**4.7**			^{2}8.4
	^{1}2.5^{1}1.7^{1}1.2	^{3}**1.2**		^{4}3.6			^{2}**41**
	^{1}2.1^{1}2.4^{1}0.83			^{4}3.6			
	^{1}1.7^{1}1.1^2**3.6**						
	^{4}**1.5**^{4}1.4^{3}0.63						
	^{3}1.0^{3}1.1^{3}1.2						
	^{3}1.1^3**1.4**^{3}1.4						
	^{3}1.2						
$N=3$							^{2}**1.9**
$N=4$	^{1}**2.0**	^{1}**0.67** ^{2}**1.8**		^{1}**1.0**			^{2}**1.7**
		^{4}0.89 ^{4}0.94		^{3}**1.5**			
		^{4}**1.1**^{3}**1.3**^{3}1.2		^{3}0.96			
		^{3}1.1^{3}1.2		^{3}1.0			
				^{3}1.5			
				^{3}1.3			
$N=5$				^{2}**1.2**			
$N=6$		^{3}**1.1**^{3}1.1				^{3}**0.89**	
$N=8$		^{2}**3.1**^{2}1.4	^{2}**0.96**			^{1}**1.3**	^{3}**1.4**
						^{2}**1.0**	^{3}1.3
						^{4}**1.2**	^{3}0.73

the total energy in the laser pulse is not affected by the phase distribution on the LC. Thus, one expects that the $S_1^+:S_2^+$ yield ratio would be enhanced by a laser pulse that is temporally broadened without excessively compromising the peak intensity. Conversely, the $S_2^+:S_1^+$ target should be maximized by a pulse shape that reduces the peak intensity without increasing the duration of the predominant temporal features in the pulse. As shown in Fig. 2, this is indeed what is observed. The best $S_1^+:S_2^+$ yield is obtained using a pulse that contains component features whose duration is longer than the 150-fs transform-limited pulse width. However, the field that is most effective in increasing the S_2^+ signal relative to S_1^+ is composed of a single short, primary pulse flanked by several smaller amplitude pulses at earlier and later times. This pulse train achieves a reduced peak intensity without increasing the duration of any of the primary subpulses. In contrast, when phase and amplitude shaping (type 2) is used, pulse duration and intensity are more easily decoupled. These results are illustrated in Fig. 3. Here we observe the optimum $S_2^+:S_1^+$ yield for a transform-limited pulse with approximately half the energy of the unshaped pulse and the maximum $S_1^+:S_2^+$ signal for a temporally broadened pulse with the full energy of the unshaped pulse.

In an attempt to determine which spectral characteristics (e.g., the observed temporal modulations) are critical for the observed level of control, we utilized a principal control analysis (PCA) method developed by White, Pearson, and Bucksbaum [25]. The Appendix provides a more complete discussion of the mathematical method employed. Principal control analysis was applied to the phase space of frequency-domain pulse parametrization with phase-only and phase and amplitude shaping control of two fragmentation yield ratios: $S_1^+:S_2^+$ and $S_2^+:S_1^+$. We found that PCA is able to reduce the dimensionality of the control space to approximately 15% of the original dimensions; the match between the optimal and reduced dimensionality FROG spectrograms can be observed in Fig. 4. This is interesting in light of some recent suggestions [20,26] that linear transformations, such

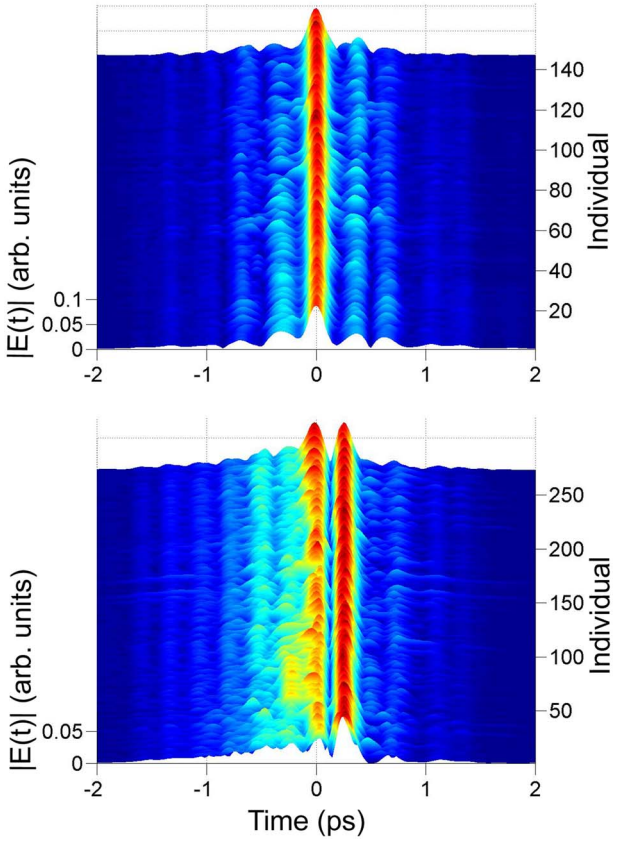

FIG. 2. (Color online) Surface plot of the magnitude of the electric field as a function of time for $S_2^+:S_1^+$ (top) and $S_1^+:S_2^+$ (bottom) optimized with a phase-only frequency domain parametrization (type 1). The plots show all individual pulse shapes with fitness $f > 0.85 f_{best}$. Generations increase from bottom to top of each plot. The uniformity of the structure in the pulse shapes over many individual pulses indicates that the GA has converged on a single solution. The color scale of the $|E(t)|$ surface is linear.

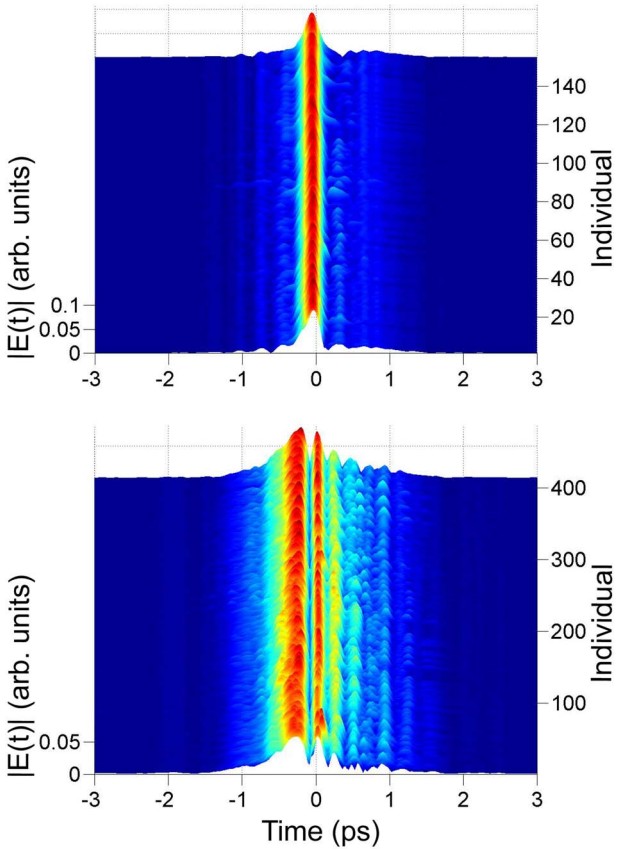

FIG. 3. (Color online) Similar to Fig. 2 for pulses optimized to maximize $S_2^+:S_1^+$ (top) and $S_1^+:S_2^+$ (bottom) but using a frequency-domain parametrization that varied both phase and amplitude (type 2).

as PCA, between bases may not be sufficient to adequately reduce the control directions needed for pulse shapes optimized for highly nonresonant multiphoton processes. Despite a lack of *a priori* knowledge of the system dynamics, a linear basis transformation yields suitable results in our case.

The PCA method assumes that the principal control directions (PCD's) are those control directions having the largest eigenvalues. We have found that the correlation of the control directions with the pulse-shape fitness may also play an important role in PCD selection. The effect of selecting the PCD's based upon eigenvalue as opposed to correlation with fitness is illustrated in Fig. 5. FROG spectrograms were reconstructed by projecting the optimal pulse shape from the GA (phase-only, $S_1^+:S_2^+$) onto a variety of essential control directions that had been selected based upon eigenvalue (left column) or correlation with fitness (right column). If the correlation with fitness of a given eigenvector also corresponded to an eigenvalue, the FROG spectrograms regenerated by each method would be identical; however, it is clear from the preservation, as well as from the spectrogram, that this is not the case. In general, PCD selection via eigenvalue yields a higher mathematical preservation than selection via correlation with fitness. This measure is purely mathematical, though, and further insight into the system dynamics may be obtained by visual examination of the pulse shapes. Selection of PCD's by correlation with fitness begins to introduce elements associated with more complex pulse shapes much sooner and always lends more intensity to the long time features than selection by eigenvalue. Comparison with the reconstructed FROG spectrograms for the phase and amplitude shaping optimization for the same yield ratio [Figs. 4(g) and 4(h)], it appears that linear and/or nonlinear chirps are indeed important pulse characteristics for controlling this system. Thus, one should be aware that there are different methods to determine the principal control directions; which method returns the essential pulse may vary, and one should not rely solely on the mathematical preservation formula.

Once the essential pulse characteristics had been identified using PCA, we compared the spectral components of the pulse to frequencies of interest in the S_8 molecule. All of the possible vibrational modes and electronic transitions [27,28] we could identify are far outside the bandwidth of our laser pulses. For example, the room-temperature vibrational modes of S_8 rings are peaked near 450 cm^{-1}, far off resonance from the laser pulse and inaccessible via impulsive Raman excitation given our 150-cm^{-1} laser bandwidth. Furthermore, since the pulse intensity varies over the focal volume, different molecules are exposed to different fields.

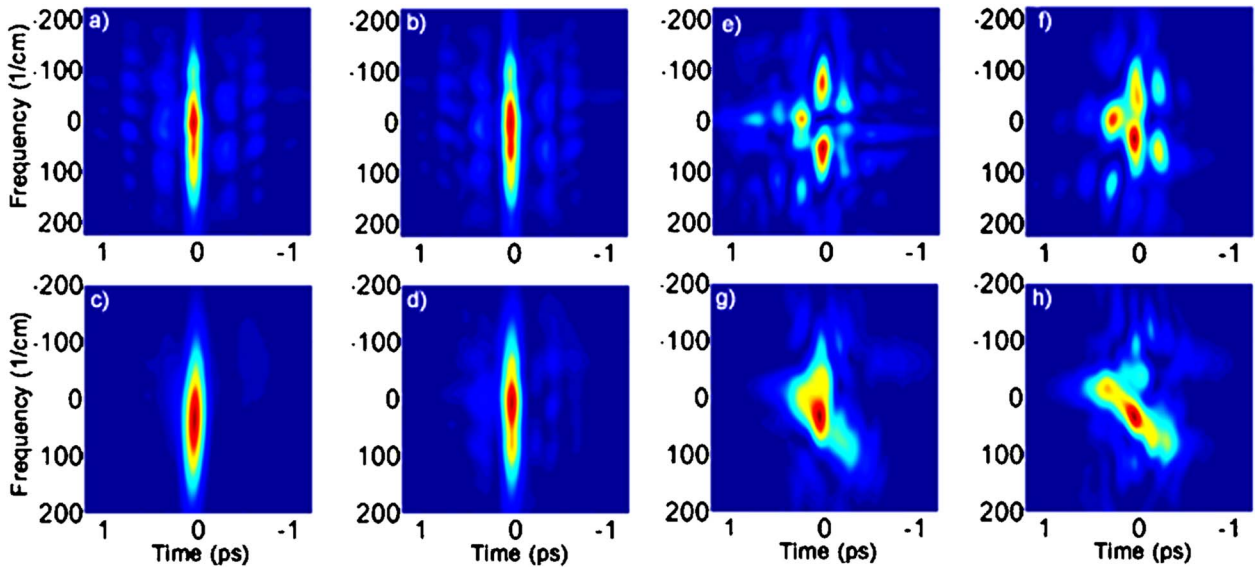

FIG. 4. (Color online) Reconstructed optimum and essential FROG spectrograms. Left block: $S_2^+:S_1^+$ ratio. Panels (a) and (b) represent the optimum and essential pulse shapes, respectively, for type-1 experiments, and panels (c) and (d) represent the same for the type-2 experiment. Right block: similar for the $S_1^+:S_2^+$ ratio. Optimum pulses are reconstructed from the genotype of the fittest pulse in the population, and the essential pulses are constructed using PCA as described in the text. The central frequency is 12658 cm^{-1}; the spectrogram frequencies are plotted relative to this point. The linear color scale goes from blue (low) to red (high). Peak values for each plot are (a) 1.0, (b) 0.91, (c) 0.70, (d) 0.20, (e) 0.55, (f) 0.33, (g) 0.33, and (h) 0.24 in arbitrary units.

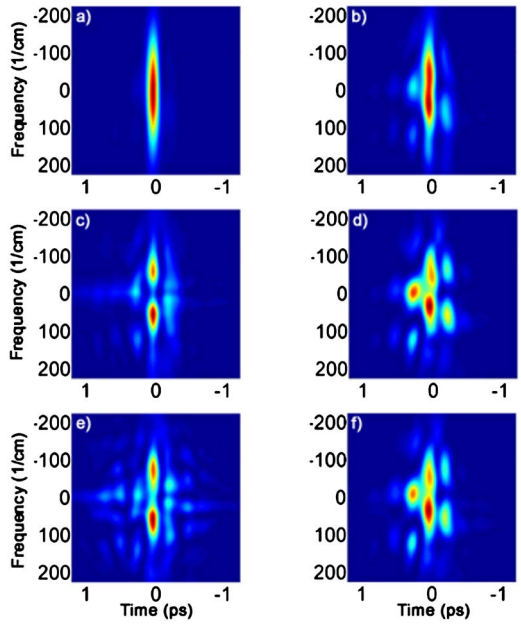

FIG. 5. (Color online) Series of reconstructed FROG spectrograms for the type-1 (phase-only), $S_1^+:S_2^+$ experiment. Left: principal control directions selected by eigenvalue for three (a), six (c), and nine (e) PCD's. Right: similar for PCD's selected by correlation with fitness. Pulse-shape preservation is as follows: (a) 46%, (b) 50%, (c) 76%, (d) 55%, (e) 95%, and (f) 69%. The optimal pulse is shown in Fig. 4(e). The linear color scale goes from blue (low) to red (high). Peak values for each plot are (a) 2.4, (b) 1.0, (c) 0.73, (d) 0.55, (e) 0.47, and (f) 0.55 in the same units as Fig. 4.

While it may be possible, given enough light and control directions, for the GA to compensate for this [29], it undoubtedly complicates the interpretation of the optimum pulse shapes. Extracting information about the fragmentation mechanism, even after using PCA to limit superfluous pulse characteristics, remains difficult.

Next, we tested the PCA results by applying a time-domain GA parametrization to the same control problems. Here individual genes are expressed as a specific property (i.e., amplitude, duration, wavelength, etc.) of one of several component pulses that are combined to produce the net temporal field. Again, two schemes, using phase-only (type-3) or phase and amplitude (type-4) shaping, have been implemented. These parametrizations take advantage of the full resolution of the pulse shaper, enabling the generation of pulses with significantly longer temporal structure and minimum spectral periodicity artifacts, while still limiting the search to 32 (or fewer) genes. Our implementation of type-3 phase-only shaping takes advantage of a Fourier-transform-based, iterative algorithm that enables fast estimation of the phase mask required to generate a specific time-dependent laser intensity distribution [30]. As shown in Table I, on average, we achieve similar gains with all four parametrizations. Interestingly, as illustrated in Fig. 6, the time-parametrization results do not show the same consistent temporal structures that appear when pixel clustering is used in the frequency-domain schemes.

Both experimental phase and amplitude (type-2 and type-4) control results and the PCA analysis suggest that pulse duration and/or spectral chirp are critical for enhancing the target yields. This begs the question: Is the control we observe for the S_1^+ and S_2^+ ion ratios due primarily to laser pulse duration and, in that sense, essentially trivial [10]? To

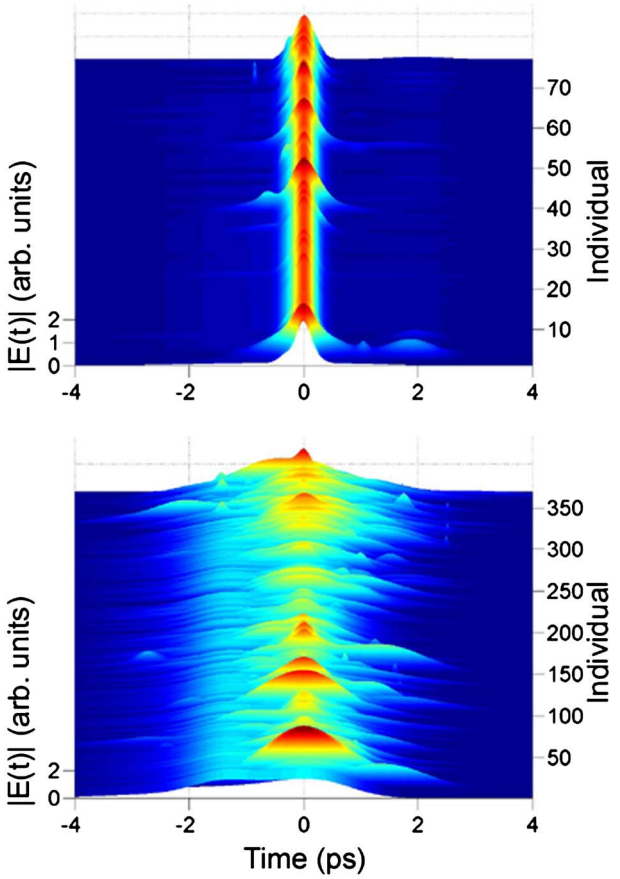

FIG. 6. (Color online) Similar to Figs. 2 and 3 except that these ratios have been optimized to maximize $S_2^+:S_1^+$ (top) and $S_1^+:S_2^+$ (bottom) using a time-domain parametrization scheme in which only the spectral phase distribution is shaped (type 3). For the particular experiments shown, the net temporal pulse is the sum of five individual pulses.

answer this question we utilized the time-domain parametrization to examine yield enhancements as a function of pulse complexity. Specifically, we ran the type-3 GA optimization for laser shapes containing one, three, five, and ten component pulses. As shown in Fig. 7, intensity distributions with higher complexity (i.e., a greater number of contributing component pulses) perform better than the single-pulse case. The corresponding pulse shapes are shown in Fig. 8.

Our time-domain measurements are consistent with the key results of the PCA. First, the precise temporal modulations found in the fittest pulses obtained from the frequency-domain parametrization are not essential for control, but some complexity is required. Second, because control can be achieved using a smaller set of appropriately chosen basis functions, many different pulse shapes which include nonessential (but nondamaging) features can be used to achieve similar yields. We also suspect, but cannot directly verify, that there are many local maxima in the multidimensional surface that defines fragment ratio yield versus laser characteristics, particularly in these focused beam experiments where ion fragments are detected from different intensity regions within the laser focal volume.

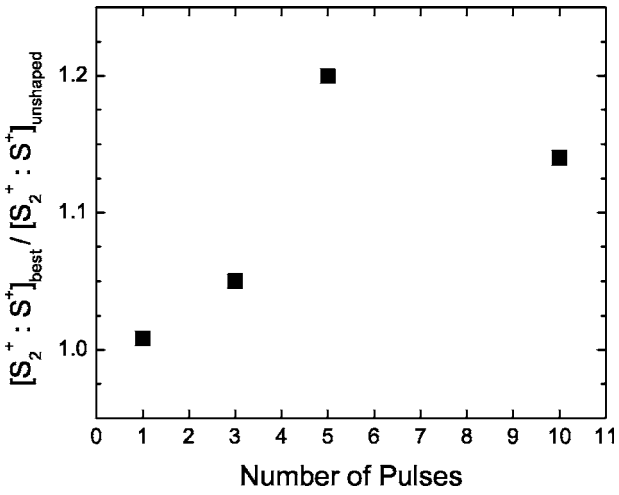

FIG. 7. Results of optimization experiments for $S_2^+:S_1^+$ as a function of pulse complexity. The pulses were generated with type-3 parametrization using one, three, five, and ten constituent pulses to arrive at the net electric field.

IV. SUMMARY

We have explored intense laser dissociative ionization of S_8 using unshaped pulses of varying duration and intensity. We have shown that closed-loop optimization of laser-pulse shapes can be used to significantly enhance the production of

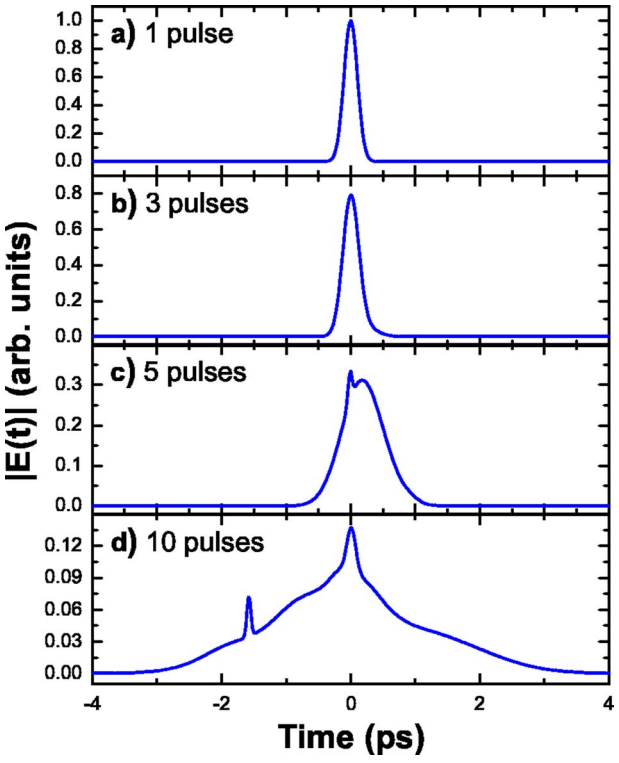

FIG. 8. (Color online) Laser-pulse shapes for the optimization of $S_2^+:S_1^+$ using type-3 parametrization using one (a), three (b), five (c), and ten (d) consitituent pulses to produce the net electric field. The scale used for the electric field is the same for each reconstructed pulse.

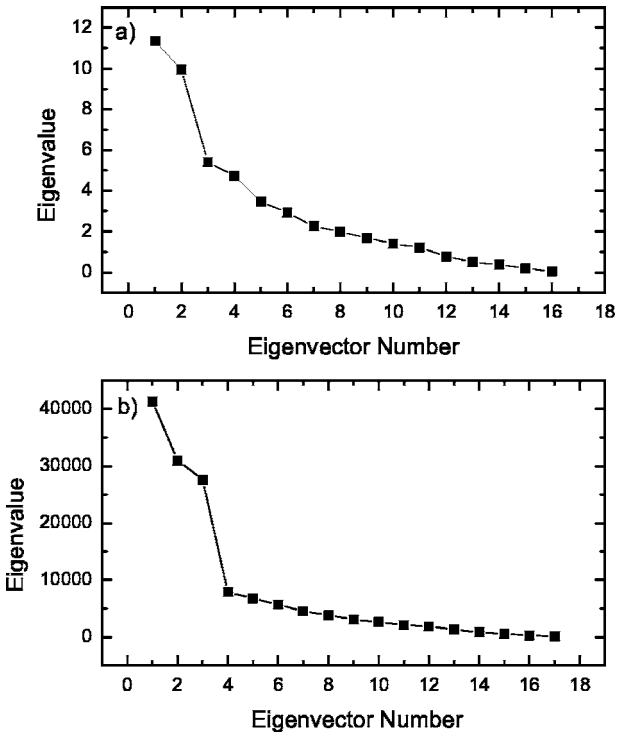

FIG. 9. Eigenvalues of the covariance matrices in descending order for the phase-only (a) and phase and amplitude (b) $S_1^+:S_2^+$ experiments.

specific target ions and ion yield ratios. We find that the implementation of multiple-pulse parametrization schemes and principal control analysis can be useful for identifying nonessential pulse characteristics when optimizing for specific targets. However, it is clear that intense laser control over such highly nonlinear processes must be hampered by intensity variation throughout the focal volume. The optimum pulse shape at one location in space will likely differ from that at other positions due to the difference in peak intensities and limitations on the total energy and frequency spectrum available in the laboratory. This effect obviously does not eliminate the possibility for substantial control. However, we believe that it does limit the gains achieved in our experiments and, perhaps more importantly, makes the identification of a specific control mechanism more difficult or impossible.

ACKNOWLEDGMENTS

The authors would like to thank Brett Pearson and James White for their discussions of PCA and M. Bajema for technical assistance in the early stages of this work. This work was supported by the Chemical Sciences, Geosciences and Biosciences Division, Office of Basic Energy Sciences, Office of Science, U.S. Department of Energy, by the National Science Foundation IGERT program under Grant No. MPS-9972790, and by the University of Virginia FEST.

APPENDIX: PRINCIPAL CONTROL ANALYSIS

White, Pearson, and Bucksbaum have applied common covariance techniques [31,32], called *principal control analysis*, to closed-loop optimal control [25]. The first step in the PCA implementation is the construction of the covariance matrix of the set of pulse shapes in the search

$$C_{ij} = \langle \delta_i \delta_j \rangle - \langle \delta_i \rangle \langle \delta_j \rangle, \tag{A1}$$

where $\delta_i = x_{i+1} - x_i$, $i = 1, \ldots, n-1$, are the nearest-neighbor phase differences, as x_i is the ith gene value and n is the number of genes in each individual. The averaging is performed over all individuals in the population. After the covariance matrix is constructed, its eigenvectors and eigenvalues λ_j are calculated. The eigenvalues are a measure of how far the algorithm moved along that eigenvector during its search. When the eigenvectors are plotted in descending order, as in Fig. 9, it is apparent that a small subset of the eigenvalues carry most of the weight of the covariance trace. In order to determine which control directions are important, we calculate the correlation of the projections of the pulse shapes onto the eigenvectors η_i with the pulse-shape fitness f.

$$B_\eta = (\langle \eta_i f \rangle - \langle \eta_i \rangle \langle f \rangle)/\sigma_{\eta_i} \sigma_f, \tag{A2}$$

where σ_{η_i} and σ_f represent the standard deviations of their respective subscripts. For comparison, a similar correlation with fitness in the original basis is also calculated:

$$B_\delta = (\langle \delta_i f \rangle - \langle \delta_i \rangle \langle f \rangle)/\sigma_{\delta_i} \sigma_f. \tag{A3}$$

When expressed in the eigenvector basis, the control directions are uncorrelated. That is, each eigenvector is an independent control direction. White *et al.* propose that the eigenvectors with the largest fitness correlation are the essential control directions u_j and expect that the eigenvectors with the largest eigenvalues will be most strongly correlated to the fitness of the pulse-shape solution [25]. Ideally, one or two eigenvectors will prove to be more strongly correlated

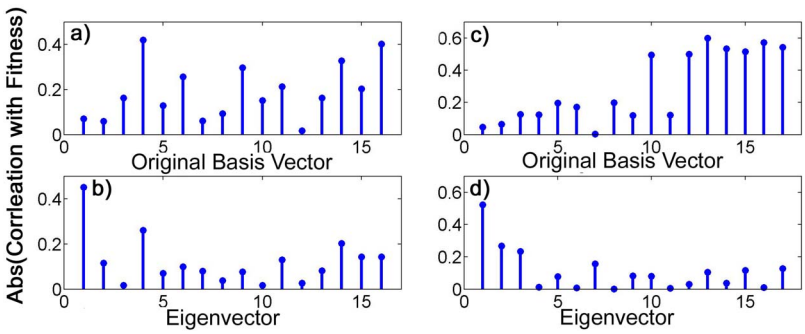

FIG. 10. (Color online) Correlation of fitness f with the original basis vectors for the phase-only (a) and phase and amplitude (c) $S_1^+:S_2^+$ experiments. Similar correlations with the control vectors in (b) and (d).

with fitness, and the remaining eigenvectors can be deemed unessential to the pulse shape and may be eliminated. We found that the eigenvectors with the largest eigenvalues are not always those most strongly correlated with fitness. Figure 10 plots the correlation with fitness versus control directions for both the original and eigenvector bases. Since the eigenvectors have been reordered in descending order, if the expectation were true, we would see a gradual decrease in the height of the stems as the eigenvector number increases. The stem plot indicates that some eigenvectors have a significant correlation with fitness despite having small eigenvalues.

The best GA solutions for each experiment are then projected onto the $k<n$ PCD's u_k, thus reducing the dimension of the control space and producing the essential pulse, $\Sigma_{j=1}^{k}\eta_j u_j(\omega)$. Ideally, this essential pulse will contain all of the traits necessary to achieve the target while minimizing irrelevant features. The mathematical extent to which the original pulse traits remain can be calculated by the preservation formula $\Sigma_{j=1}^{k}\eta_j{}^2(\omega)$.

[1] M. J. DeWitt and R. J. Levis, J. Chem. Phys. **102**, 8670 (1995).
[2] M. J. DeWitt, D. W. Peters, and R. J. Levis, Chem. Phys. **218**, 211 (1997).
[3] K. W. D. Ledingham, R. P. Singhal, D. J. Smith, T. McCanny, P. Graham, H. S. Kilic, W. X. Peng, S. L. Wang, A. J. Langley, P. F. Taday, and C. Kosmidis, J. Phys. Chem. A **102**, 3002 (1998).
[4] D. J. Smith, K. W. D. Ledingham, R. P. Singhal, H. S. Kilic, T. McCanny, A. J. Langley, P. F. Taday, and C. Kosmidis, Rapid Commun. Mass Spectrom. **12**, 813 (1998).
[5] A. M. Weiner, D. E. Leaird, J. S. Patel, and J. R. Wullert, Opt. Lett. **15**, 326 (1990).
[6] M. M. Wefers and K. A. Nelson, Opt. Lett. **18**, 2032 (1993).
[7] R. S. Judson and H. Rabitz, Phys. Rev. Lett. **68**, 1500 (1992).
[8] B. J. Pearson, J. L. White, T. C. Weinacht, and P. H. Bucksbaum, Phys. Rev. A **63**, 063412 (2001).
[9] D. Zeidler, S. Frey, K.-L. Kompa, and M. Motzkus, Phys. Rev. A **64**, 023420 (2001).
[10] R. J. Levis, G. M. Menkir, and H. Rabitz, Science **292**, 709 (2001).
[11] A. Assion, T. Baumert, M. Bergt, T. Brixner, B. Kiefer, V. Seyfried, M. Strehle, and G. Gerber, Science **282**, 919 (1998).
[12] M. Bergt, T. Brixner, B. Kiefer, M. Strehle, and G. Gerber, J. Phys. Chem. A **103**, 10381 (1999).
[13] *NIST Chemistry WebBook*, NIST Standard Reference Database 69, edited by P. J. Linstrom and W. G. Mallard (National Institute of Standards and Technology, Gaithersburg, MD, 2001), http://webbook.nist.gov
[14] J. M. Geremia, W. Zhu, and H. Rabitz, J. Chem. Phys. **113**, 10841 (2000).
[15] T. Hornung, M. Motzkus, and R. de Vivie-Riedle, Phys. Rev. A **65**, 021403(R) (2002).
[16] I. R. Sola and H. Rabitz, J. Chem. Phys. **120**, 9009 (2004).
[17] T. Hornung, R. Meier, and M. Motzkus, Chem. Phys. Lett. **326**, 445 (2000).
[18] H. A. Rabitz, M. M. Hsieh, and C. M. Rosenthal, Science **303**, 1998 (2004).
[19] G. Turinici and H. Rabitz, Phys. Rev. A **70**, 063412 (2004).
[20] F. Langhojer, D. Cardoza, M. Baertschy, and T. Weinacht, J. Chem. Phys. **122**, 014102 (2005).
[21] J. Berkowitz, in *Elemental Sulfur*, edited by Beat Mayer (Wiley Interscience, New York, 1965), Chap. 7.
[22] E. Wells, M. J. DeWitt, and R. R. Jones, Phys. Rev. A **66**, 013409 (2002).
[23] David E. Goldberg, *Genetic Algorithms in Search, Optimization, and Machine Learning* (Addison-Wesley, Boston, 1989).
[24] R. Trebino, K. W. DeLong, D. N. Fittinghoff, J. N. Sweetser, M. A. Krumbuegel, and D. J. Kane, Rev. Sci. Instrum. **68**, 3277 (1997).
[25] J. L. White, B. J. Pearson, and P. H. Bucksbaum, J. Phys. B **37**, L399 (2004).
[26] D. Cardoza, D. Trallero-Herrero, F. Langhojer, H. Rabitz, and T. Weinacht, J. Chem. Phys. **122**, 124306 (2005).
[27] R. O. Jones and P. Ballone, J. Chem. Phys. **118**, 9257 (2003).
[28] M. H. Wong, Y. Steudel, and R. Seudel, Chem. Phys. Lett. **364**, 387 (2002).
[29] K. Sundermann, H. Rabitz, and R. de Vivie-Riedle, Phys. Rev. A **62**, 013409 (2000).
[30] M. Hacker, G. Stobrawa, and T. Feurer, Opt. Express **9**, 191 (2001).
[31] I. T. Jolliffe, *Principal Component Analysis*, 2nd ed. (Springer, Berlin, 2002).
[32] B. Kolman and D. R. Hill, *Elementary Linear Algebra*, 7th ed. (Prentice-Hall, Englewood Cliffs, NJ, 1999).